

WATER IN COMET C/2003 K4 (LINEAR) WITH *SPITZER*

CHARLES E. WOODWARD¹, MICHAEL S. KELLEY^{1,2},
DOMINIQUE BOCKELÉE-MORVAN³,
R. D. GEHRZ¹

ABSTRACT

We present sensitive 5.5–7.6 μm spectra of comet C/2003 K4 (LINEAR) obtained on 16 July 2004 ($r_h = 1.760$ AU, $\Delta_{\text{Spitzer}} = 1.409$ AU, phase angle 35.4°) with the *Spitzer* Space Telescope. The ν_2 vibrational band of water is detected with a high signal-to-noise ratio ($\gtrsim 50$). Model fitting to the best spectrum yields a water ortho-to-para ratio of 2.47 ± 0.27 , which corresponds to a spin temperature of $28.5^{+6.5}_{-3.5}$ K. Spectra acquired at different offset positions show that the rotational temperature decreases with increasing distance from the nucleus, which is consistent with evolution from thermal to fluorescence equilibrium. The inferred water production rate is $(2.43 \pm 0.25) \times 10^{29}$ molec. s⁻¹. The spectra do not show any evidence for emission from PAHs and carbonate minerals, in contrast to results reported for comets 9P/Tempel 1 and C/1995 O1 (Hale-Bopp). However, residual emission is observed near 7.3 μm the origin of which remains unidentified.

Subject headings: Comets: individual (C/2003 K4 LINEAR): infrared: solar system

¹Department of Astronomy, School of Physics and Astronomy, 116 Church Street, S. E., University of Minnesota, Minneapolis, MN 55455, *chelsea@astro.umn.edu*, *gehrz@astro.umn.edu*

²Current address: Department of Physics, University of Central Florida, 4000 Central Florida Blvd., Orlando, FL 32816-2385, *msk@physics.ucf.edu*

³LESIA, Observatoire de Paris, 5 place Jules Janssen, F92195, Meudon, France, *dominique.bockelee@obspm.fr*

1. INTRODUCTION

The composition of cometary nuclei probes the physical conditions in the early solar nebula, the survival of materials from the interstellar medium (ISM), and the cold dense molecular cloud core in which the solar system formed (Wooden et al. 2004; Ehrenfreund et al. 2004; Mumma et al. 2003). Comet nuclei are highly porous agglomerates of ice and dust grains, perhaps with highly stratified, inhomogeneous layers of varied density, porosity, and composition (Harker et al. 2007; Belton et al. 2006; Oró et al. 2006; A’Hearn et al. 2005; Prialnik et al. 2004). The nucleus composition is dominated by ices (primarily water), organic refractory materials, silicates, and carbonaceous materials. When comets are within heliocentric distances of $r_h \leq 20$ AU, solar insolation triggers sublimation and the release of volatile gases, sometimes sporadically, forming observable comae (Meech & Sovern 2004).

In the nucleus of a comet, volatiles are frozen as ices or trapped as gases in amorphous water ice (Capria 2002; Prialnik 2002). Cometary activity occurs when gases are released through sublimation or through the exoergic crystallization of amorphous water ice. Between ~ 20 to 5 AU, when nuclear surface temperatures reach $\simeq 20 - 100$ K, CO ice sublimates from the nucleus (Capria et al. 2000; Prialnik 2002), possibly from near the surface (Gunnarsson et al. 2003), and triggers activity and intermittent outbursts. Between ~ 6 to ~ 4 AU, a dramatic increase occurs in gas production and grain entrainment and signals the coma onset stage. At nuclear surface temperatures of $\sim 120 - 130$ K (Prialnik et al. 2004), the water ice phase transition (amorphous to crystalline) releases a fraction of the trapped volatile gases. Strong erosion maintains the CO-ice sublimation and phase transition fronts relatively close to the surface (Capria et al. 2000). At ~ 4 to ~ 3 AU, the near-surface crystalline water ice layer, with its remaining trapped gases, begins to sublime. Water sublimation drives this vigorous activity stage that is often characterized by discrete active areas or jets.

Water is the dominate ice in comet nuclei and the production rate of water is correlated with comet activity. It influences the thermal balance of the coma as a strong coolant. At some wavelengths $\leq 10 \mu\text{m}$ emission from ro-vibrational transitions of water can dominate the spectral energy distribution (Crovisier et al. 1997b); water can also be observed from its rotational transitions at submillimeter wavelengths (see review of Bockelée-Morvan et al. 2004). Probed through spectroscopic observations of coma species, the water production rate, coma temperature, and the nuclear spin temperatures derived from ortho-to-para ratios (OPR) are of particular interest in the study of cometary atmospheres and cometary physics. These physical characteristics, complemented by knowledge of the nucleus refractory and ice composition, provide constraints on solar nebula models (Mumma et al. 2003; Markwick & Charnley 2005), and restrict the formation zones within the protoplanetary disk

where cometary nuclei could conglomerate. In particular, the nuclear spin temperature of water measured in comet comae may be indicative of the chemical formation temperature of water (Dello Russo et al. 2005; Mumma et al. 1993) therefore identifying the environment where pre-cometary ices condensed.

Here we present longslit *Spitzer Space Telescope* spectroscopic observations of the $6\ \mu\text{m}$ ν_2 vibrational band of water detected in comet C/2003 K4 (LINEAR) at $r_h = 1.760$ AU. The high signal-to-noise and the Infrared Spectrograph (IRS) longslit enable us to extract spatially resolved spectra in the coma and to measure the water production rate, $Q(\text{H}_2\text{O})$, and the rotational temperature, T_{rot} , and the OPR variation in the coma. Space observations of the strong ν_2 fundamental bands near $6\ \mu\text{m}$ present a potentially more advantageous method for constraining water production rates and T_{rot} in comets than the more common ground-based measurement of the weaker non-resonance fluorescent “hot-bands” near $2.9\ \mu\text{m}$ as the complex corrections for telluric extinction, slit-loss due to seeing, and consideration of whether the local radiative pump in the coma is optically thick are minimized (Bonev et al. 2007, 2006; Dello Russo et al. 2004; Bockelée-Morvan 1987). In addition, accurate laboratory measurements of the absorption line strengths used to compute Einstein coefficients, $A_{\nu',\nu''}(\text{s}^{-1})$, for the ν_2 pump from the ground-state (000) are extant (Barber et al. 2006; Dello Russo et al. 2004; Partridge & Schwenke 1997) while those for the hot bands are more challenging, leading to some uncertainty in estimates of the spontaneous emission rates, $g_{\nu',\nu''}(\text{s}^{-1})$.

The infrared ν_2 band of water was first detected with the Short Wavelength Spectrometer (SWS) of the *Infrared Space Observatory* (ISO) in the exceptional comet C/1995 O1 (Hale-Bopp) at $r_h \simeq 2.9$ AU (Crovisier et al. 1997a). The SWS spectral resolution of ~ 1000 resulted in the detection of several individual ro-vibrational lines. However, the low signal-to-noise ratio prevented detailed analysis of their relative intensities. We discuss the *Spitzer* observations and data reduction techniques in § 2. Section 3.1 discusses the modeling of the ν_2 water band. Section 3.2 through § 3.5 present the results, followed in § 4 by a discussion of residual emission features, including a comparison with the ν_2 band of water detected in other comets with *Spitzer*. Section 5 presents a summary of our study of comet C/2004 K4 (LINEAR).

2. OBSERVATIONS AND REDUCTION

First identified as an asteroidal object in the LINEAR survey, C/2003 K4 (LINEAR) was discovered to have an extended spherical coma by Young & McGaha (2004) with parabolic orbital elements consistent with that of a dynamically new Oort Cloud comet. The following

year upon perihelion approach ($q = 1.02$ AU, 2004 Oct 13.5 UT), C/2003 K4 (LINEAR) was bright in the optical ($V \lesssim 7$ mag) and was noted to exhibit a primarily featureless $10\ \mu\text{m}$ spectral energy distribution with emission from large amorphous carbon and silicate grains (grain radii $\geq 0.7\ \mu\text{m}$) dominating the coma (Woodward et al. 2004). The $10\ \mu\text{m}$ silicate feature-to-continuum ratio was observed to be near unity (Sitko et al. 2004; Russell et al. 2004), with little evidence for structure near $11.2\ \mu\text{m}$ attributable to Mg-rich crystalline olivine grains (Sitko et al. 2004; Woodward et al. 2004). Schulz, Stüwe, & Erd (2005) observed a single broad coma feature in broadband images, perpendicular to the sunward direction in C/2003 K4 (LINEAR) during the 2004 May through 2004 July period with an increase in the amount of inferred gas-contamination in the B and V coma surface brightness with decreasing heliocentric distance. During the epoch of our *Spitzer* observations (§ 2.1), the comet produced a considerable amount of dust ($Af\rho \simeq 10,000\ \text{cm}$; Schulz, Stüwe, & Erd 2005).

2.1. *Spitzer* IRS

Spectra of comet C/2003 K4 (LINEAR) were obtained with the Infrared Spectrograph (IRS) instrument (Houck et al. 2004) on the *Spitzer Space Telescope* (Gehrz et al. 2007; Werner et al. 2004). The comet was observed in the second order of the short-wavelength, low-resolution module (SL2) on 2004 Jul 16 at 04:56 UT as part of a *Spitzer* Guaranteed Time Observation (GTO) program (PI: R.D. Gehrz), program identification (PID) 131, astronomical observation request (AOR) key 0008525056, and processed with IRS reduction pipeline S15.3.0. The SL2 slit is $3.7''$ wide and provides $57''$ of spatially resolved spectra ($1.8''\ \text{pixel}^{-1}$) with a spectral dispersion of $0.06\ \mu\text{m}$. Six spectra ($14\ \text{s} \times 3$ cycles) at 5.2 – $7.6\ \mu\text{m}$ were recorded in a 3×2 spectral map, with $7.2'' \times 78''$ steps (perpendicular \times parallel to the long slit dimension). The comet was at a heliocentric distance (r_h) of 1.760 AU, a *Spitzer*-comet distance of 1.409 AU, and a phase angle of 35.4° .

At the time of acquisition, we attempted to acquire the comet nucleus with the *Spitzer* IRS $15\ \mu\text{m}$ peak-up array. However, the bright inner coma saturated a $76'' \times 64''$ ellipse in the $98'' \times 72''$ peak-up array preventing the spacecraft from computing a centroid on the comet. Thus, the telescope pointed to the comet’s nominal ephemeris position derived from orbital elements uploaded to the spacecraft prior to the execution of the AOR. On the date of observation, 2004 Jul 16 UT, the nominal position of the comet derived from these elements was $28''$ from the actual position calculated with revised elements from JPL ephemeris #96 (computed 2006 Dec 14 with a data-arc spanning from 2003 May 28 through 2006 Nov 17). However, comet C/2003 K4 (LINEAR) had an extensive coma ($\geq 1'$ in diameter) at the

epoch of our *Spitzer* observation and thus error in the position of the nucleus did not affect our ability to obtain spectra of the comet coma. Our discussion of the IRS slit positions within the coma of the comet are referenced to the actual position as computed from the most recent JPL ephemeris. Figure 1 shows the blue peak-up image (saturated core), the slit positions, and the position of the nucleus (*cross*).

Coma emission (including the spectral signature from water lines) is present in all portions of our slits to varying degrees. Therefore, a robust estimate of the background emission is difficult to accurately assess (to the level of a few percent) using the *Spitzer* longslit observations of comet C/2003 K4 (LINEAR) alone. However, in the same IRS campaign (#10) an observation with the same IRS AOR parameters toward a similar ecliptic latitude ($52.5^\circ \pm 0.5^\circ$) was available. The background derived from this IRS observation (AOR key 0004733952 obtained from the *Spitzer* archive) was two-dimensionally subtracted from the basic calibrated data products (BCDs) of comet C/2003 K4 (LINEAR).

After background subtraction, we corrected the world coordinate system of the two-dimensional spectral frames for the motion of the comet, then combined each source observation into data cubes with the CUBE Builder for IRS Spectra Maps (CUBISM, Smith et al. 2007) program (v1.5)¹. CUBISM combines each cycle and each slit position into a data cube where two axes contain the spatial information ($1.85''$ pixel⁻¹ grid), and the remaining axis contains the spectral information. A separate cube is created for the pipeline errors derived from the individual BCDs. The program photometrically calibrates the data, including a correction for diffraction losses at the entrance slit (the so-called slit-loss correction factor; Kelley et al. 2006; Spitzer Science Center 2006).

IRS spectra extracted from SL2 module have weak fringing artifacts ($\lesssim 2\%$ of the source flux, $F(\lambda_i)$, at a given wavelength) that are difficult to completely remove using a sinusoidal function, as they are not spectrally resolved and vary with position in the slit (Spitzer Science Center 2006). Thus, to account for any potential residual fringe contamination we compute the flux uncertainty in our extracted spectra at a given wavelength from the quadrature sum of the photometric error arising from the pipeline processing of individual BCDs plus a contribution due to SL2 fringing signal equal to $0.02 \times F(\lambda_i)$. This latter term is an *upper limit* to the fringe uncertainty.

We extracted spectra from nine locations in the coma, as shown in Fig. 1. The extraction apertures are $1.85'' \times 7.40''$ rectangles (subtending $1890 \text{ km} \times 7560 \text{ km}$ within the coma). We restricted our nine source extractions and subsequent analysis to locations where the coma is brightest, from $0''$ to $+30''$ offset from the nucleus (Fig. 1).

¹Available at <http://ssc.spitzer.caltech.edu/archanaly/contributed/cubism/>

2.2. Wavelength Calibration

The water lines are unresolved and blended in the IRS spectra. Furthermore, the *Spitzer* IRS spectra are calibrated with standards measured near the center of the slit and three of our extractions occur near the slit edge. Analysis of the wavelength calibration and unresolved line widths is critical for identifying and fitting the water lines in the IRS spectra. To verify the wavelength calibration at the slit edge, we reduced IRS calibration observations of NGC 7027 at the center and edge of the SL2 slit. The NGC 7027 observations (AOR key 0010066432, *Spitzer* PID 1410, IRS pipeline S13.2.0) were taken during the same IRS observing campaign (IRS#10) as the C/2003 K4 (LINEAR) spectra. We fit Gaussians to the [Mg V] $5.61\ \mu\text{m}$ line (Bernard Salas et al. 2001) with the nebula at the center and edge positions. The width of the [Mg V] line in NGC 7027 at the center position agrees with the spectral resolution solution provided by the *Spitzer* Science Center ($0.0605\ \mu\text{m}$). At the edge position, the line width increases to $0.0655 \pm 0.0002\ \mu\text{m}$. The [Mg V] line was observed at a central wavelength of $5.6242 \pm 0.0003\ \mu\text{m}$. Accounting for Doppler shift, the observed wavelength is $0.0137 \pm 0.0007\ \mu\text{m}$ from the vacuum rest wavelength of $5.6099 \pm 0.0006\ \mu\text{m}$. The IRS SL2 wavelength calibration is $\pm 0.006\ \mu\text{m}$ (r.m.s.), indicating the [Mg V] shift is $2.3\text{-}\sigma$ from the expected central wavelength. The Gaussian fits show no significant difference in central wavelength between the center and edge positions. We compare the wavelength positions of the water lines to the expected central wavelengths in § 3.

3. THE ν_2 WATER BAND IN COMET C/2003 K4 (LINEAR)

3.1. Model Fitting

At the resolution of the SL2 *Spitzer* spectrometer ($R \approx 100$), the ν_2 water band shows ro-vibrational structure from which information on the rotational temperature, T_{rot} , in the ground vibrational state can be obtained. Though the spectral resolution is not high enough to separate individual ro-vibrational lines, and therefore ortho from para water lines, it is still possible to assess whether our *Spitzer* spectra can provide some constraints on the OPR. Previous determinations of the OPR in cometary water were based on water infrared spectra obtained with resolving powers between 1500 and 25000 (e.g., Mumma et al. 1993; Crovisier et al. 1997b; Dello Russo et al. 2005; Kawakita et al. 2006; Bonev et al. 2007).

Vibrational emission from cometary parent molecules results from radiative excitation by solar infrared radiation followed by fluorescence. For the fundamental vibrational bands of water, including ν_2 , emission is not pure resonant fluorescence, as these bands are significantly populated by radiative decay from higher excited vibrational states. The vibrational

fluorescence scheme of cometary water is presented by Bockelée-Morvan & Crovisier (1989). The ν_2 band is significantly populated by decay of the $\nu_2 + \nu_3$ band. The resulting emission rate of ν_2 is $2.41 \times 10^{-4} \text{ s}^{-1}$ at $r_h = 1 \text{ AU}$ from the Sun. The $\nu_2 + \nu_3 - \nu_3$ hot band has an emission rate of $7.4 \times 10^{-6} \text{ s}^{-1}$ and therefore does not contribute significantly to the emission observed between 6 and 7 μm . Other hot bands (e.g., $(\nu_1 + \nu_2 + \nu_3) - (\nu_1 + \nu_3)$) are even weaker.

We used the model of fluorescence water emission presented by Bockelée-Morvan & Crovisier (1989) for analyzing the *Spitzer* data. This model considers five excited vibrational states and their subsequent radiative cascades, and is an improvement of that presented in detail in Bockelée-Morvan (1987), where only the ν_2 and ν_3 bands are considered. Einstein coefficients for ro-vibrational transitions are computed using the 2003 edition of the GEISA spectroscopic database (Jacquinet-Husson et al. 2005), which includes all significant routes leading to ν_2 excitation, including via hot bands. Comparison of the line strengths given in GEISA with those resulting from the *ab-initio* calculations of Partridge & Schwenke (1997) verified that the line-by-line relative intensities are insensitive (within 3–4%) to the choice of water line lists.

Our water model takes into account opacity effects in vibrational excitation and emission, using the escape probability formalism. For computing the line-by-line fluorescence, we considered 32 ortho and 32 para rotational levels in each vibrational state. The rotational populations in the ground vibrational state can be described by a Boltzmann distribution at a temperature T_{rot} , or the populations can be computed using an excitation model that considers the evolving excitation conditions experienced by the water molecules as they expand in the coma (§ 3.3). In this detailed model, ro-vibrational line intensities are computed for a circular aperture centered on the nucleus. We do not expect the results to be significantly sensitive to the shape of the aperture, providing the aperture area is conserved. From the model output, synthetic *Spitzer* spectra were generated by convolving the intensity of the individual ro-vibrational lines with the instrumental spectral response of the spectrometer, described by a Gaussian. Figure 2 shows examples of synthetic spectra obtained for the spectral resolution of SL2 and a 15 times higher resolving power. At first glance, the position and relative intensities of the peaks in the water modeled spectrum match approximately those in the C/2003 K4 (LINEAR) *Spitzer* spectra shown in Fig. 3, thereby demonstrating that these spectra are dominated by water emission.

For fitting the observed spectra, we assumed that the rotational populations of the ground vibrational state follow a Boltzmann distribution. The gas expansion velocity, v_{exp} , was fixed to 0.8 km s^{-1} . The water photodissociation rate was taken equal to $1.6 \times 10^{-5} \text{ s}^{-1}$ ($r_h = 1 \text{ AU}$). This rate takes into account the solar activity at the time of the observations

following the formalism described by Crovisier (1989). The only free parameters of the model are the water production rate $Q(\text{H}_2\text{O})$, T_{rot} , and the OPR.

Overall, opacity effects are small. We computed that they affect the total intensity of the ν_2 band by 6% for the spectrum of C/2003 K4 (LINEAR) acquired closest to the nucleus (7.2'' offset, Fig. 1). In addition, if opacity effects are not properly taken into account in the calculations, then the derived OPR also can be underestimated (on the order of $\sim 6\%$).

The water band emission is in excess of the dust continuum emission (Fig. 3). In the first analyses, the underlying continuum was determined using a 5-th order polynomial fit, and the residual (continuum-subtracted) spectra were fit with the water model, applying a least-squares method that uses the gradient-search algorithm of Marquardt. Continuum subtraction was not completely satisfactory, as excess continuum emission remained near 6.26 μm , while the ν_2 band is almost free of lines at this wavelength (Fig. 2). More robust fits could be obtained by fitting simultaneously the underlying continuum and the water emission. Thus, we fit the original spectra with a composite curve consisting of the modeled water spectrum superimposed on a polynomial. Polynomials of 5- or 6-degree were used. However, final results were not found to be significantly sensitive to the choice of the polynomial degree between 3 and 6.

The nominal spectral resolution of SL2 is 0.060 μm near 6 μm . Model fits to the best C/2003 K4 (LINEAR) spectrum (7.2'' offset) with the spectral resolution left as a free parameter yielded $\Delta\lambda = 0.067 \pm 0.004$ μm , agreeing with the edge observation of NGC 7027 (§ 2.2). Results of model fits given in Table 1 were obtained with $\Delta\lambda$ fixed to 0.065 μm . However, almost identical results (within the error) are returned with $\Delta\lambda = 0.060$ μm . For example, for the highest signal-to-noise ratio spectrum (Fig. 3, box A), the retrieved OPR is changed from 2.47 ± 0.27 to 2.31 ± 0.24 . We also found that the frequency calibration in SL2 spectra is likely incorrect by a tenth of the resolving power. The central wavelengths of ν_2 band structures in C/2003 K4 (LINEAR) spectra are better matched by shifting the observed spectra by 0.0032 to 0.0062 μm , within the errors discussed in § 2. For example, for the 7.2'' offset spectrum, the χ^2 between 5.8 and 7.1 μm is decreased by a factor 2.8 when applying a 0.0062 μm offset. The spectra of comet C/2003 K4 were shifted by 0.0032 to 0.0062 μm for the model fits shown in Table 1 and the corresponding figures (Figs. 3 and 4).

3.2. Water Modeling Results

The best-fit modeled spectra for comet C/2003 K4 (LINEAR) are shown in Figs. 3 and 4, where in the latter figure the continuum has been subtracted. Residuals with respect

to observed spectra are shown in the bottom of Fig. 4. Retrieved model parameters are given in Table 1. The agreement between our models and the *Spitzer* spectra is rather good for slit extractions A, D, and G, with reduced χ^2 less than 1 (Table 1).

Some excess emission ($> 3\text{-}\sigma$ deviation) is noticeable at $6.05\text{ }\mu\text{m}$ in most of the spectra at offset $> 18''$. Models that incorporate values of T_{rot} higher than those determined from model fitting (Table 1) reduce the residual continuum emission near $6.05\text{ }\mu\text{m}$ but are inconsistent with the relative water line intensities arising from intrinsically stronger lines (Fig. 2) measured longward $6.3\text{ }\mu\text{m}$. The variation in emergent water line intensities for $20 < T_{rot}(\text{K}) < 90$ which produce the broad emission feature from 5.5 to $7.0\text{ }\mu\text{m}$ when the models are convolved to the resolution of the *Spitzer* IRS SL2 are shown in Fig. 5. The $6.05\text{ }\mu\text{m}$ peak (mainly ortho $2_{12}\text{-}1_{01}\text{ }\nu_2$ line) is more intense than the $6.18\text{ }\mu\text{m}$ (mainly $1_{10}\text{-}1_{01}$ line) peak only for high T_{rot} ($> 60\text{ K}$). At low T_{rot} , these two lines result essentially from IR pumping from the 1_{01} ground state rotational level: the ratio of their intensities $I(6.18\text{ }\mu\text{m})/I(6.05\text{ }\mu\text{m})$ then depends uniquely on ro-vibrational Einstein A -coefficients and is predicted to be 1.5.

Weak residual emission ($2\text{-}\sigma$ deviation) is also observed at $5.90\text{--}5.95\text{ }\mu\text{m}$ (see B, E, H extractions in Fig. 3). This excess emission does not coincide in wavelength to the position of the $5.88\text{ }\mu\text{m}$ peak of the water band, and may be related to flaws in background subtraction.

Our derived values of T_{rot} and OPR could be affected by the residual emission present between $5.90\text{--}6.1\text{ }\mu\text{m}$. This emission (in excess of fringe artifact contamination) may arise from sources of weak line and continuum emission other than water not accounted for in our models. To quantify such effects, we derived estimates of T_{rot} and OPR by independently fitting two partial subsections of the spectra ($5.85\text{--}6.3\text{ }\mu\text{m}$ and $6.3\text{--}7.0\text{ }\mu\text{m}$) and any continua shortward of $5.8\text{ }\mu\text{m}$ and longward of $7.0\text{ }\mu\text{m}$ for the brightest slit extractions. These independent model fits, including those derived from the best reduced χ -squared fit of the entire spectra, are summarized in Table 2. Consistent OPR values are obtained from the independent model fits. The derived T_{rot} values are higher as a result of the $5.90\text{--}6.1\text{ }\mu\text{m}$ excess flux only when the $5.85\text{--}6.3\text{ }\mu\text{m}$ part of the spectrum is considered. Table 1 provides model parameters for all slit extractions retrieved by fitting the $6.3\text{--}7.0\text{ }\mu\text{m}$ part of the water spectrum. However, these latter fit parameters are not significantly different from those derived by fitting the entire spectrum.

3.3. Rotational Temperature

The inferred rotational temperatures are between 18 and 34 K and tend to decrease with increasing distance from the nucleus (Fig. 6). The rotational temperatures are not constant with respect to cometocentric distance out to 3×10^4 km within the uncertainties. A linear least squares fit to T_{rot} in Table 1, as a function of distance to nucleus, gives a slope of $-(6.1 \pm 2.2) \times 10^{-4}$ K km $^{-1}$. Such behavior is expected. In the inner coma, collisions are important and the rotational levels of the fundamental vibrational state are thermalized at the local temperature. However, in the outer coma radiative pumping prevails and the rotational population of the water molecules reaches a cold fluorescence equilibrium (e.g., Bockelée-Morvan 1987). How the populations evolve from thermal to fluorescence equilibrium depends of the density of the collisional partners, and related collisional cross-sections. Other attempts to examine the variation in water rotational temperature with cometocentric distance (Bonev et al. 2007) are restricted to the inner ($\lesssim 10^3$ km) collision-dominated coma.

Water excitation models currently developed by various investigators include both H₂O-H₂O and H₂O-e⁻ collisions (Biver 1997; Bensch & Bergin 2004; Zakharov et al. 2007). For our analysis, we use the excitation model of Biver (1997), which differs from the models of Bensch & Bergin (2004) and Zakharov et al. (2007) by the method used to solve radiation trapping effects, but yields almost similar results (Zakharov et al. 2007). The electron density and radial temperature distribution is based on the measurements of 1P/Halley made by the Giotto mass spectrometers (e.g., Eberhardt & Krankowsky 1995), to which scaling factors are applied to account for variations with water production rate and heliocentric distance. The parameter x_{ne} is a multiplying factor to the electron density, normalized to the 1P/Halley Giotto measurements ($x_{ne}(1P/Halley) = 1$). The output of the model is the rotational populations in the ground vibrational state as a function of distance to nucleus. The populations are included in the water infrared fluorescence model to simulate water spectra at offset positions. For direct comparison with the observations, rotational temperatures are derived by fitting the synthetic spectra, as was done for the observed spectra.

Figure 6 shows the evolution of T_{rot} predicted for x_{ne} values of 0.2, 0.5, and 1.0, and inner coma kinetic temperatures T_{kin} of 30, 40, 50, and 100 K. These values of the x_{ne} parameter were selected because the electron density is rather uncertain and mapping of the 557 GHz H₂O line favors $x_{ne} \sim 0.2$ (Biver et al. 2007). The predicted increase in T_{rot} at ~ 2000 km offset is due to thermal excitation by hot electrons. In the electron density model, this distance corresponds to the contact surface, R_{CS} , where the electron temperature and density undergo a steep increase (Xie & Mumma 1992). Beyond $\sim 2R_{CS}$, T_{rot} decreases because the effect of excitation by electronic collisions become less efficient with respect to radiative decay

and the fluorescence equilibrium of the ground vibrational state is cold. In the 7000–15000 km region, the model predicts a decrease in T_{rot} of $\Delta T_{rot} = 6$ to 11 K for the considered parameters, in contrast to the observed decrease of ~ 5 to 6 K. If one considers uncertainties associated with T_{rot} derived from the *Spitzer* spectra, models with $T_{kin} = 30 - 90$ K and $x_{ne} = 0.2 - 0.5$ are satisfactory. A x_{ne} value of 1.0 does not fit the data obtained at 7.2'' offset (Fig. 6), in agreement with Biver et al. (2007). The kinetic temperature is poorly constrained at the sampled cometocentric distances because, T_{rot} retains little memory of excitation conditions prevailing in the collisional region.

3.4. Ortho-to-Para Ratio

Though the spectral resolution of the SL2 spectra is low ($R \approx 100$), model fitting provides an accurate measurement of the OPR in comet C/2003 K4 (LINEAR) for the high signal-to-noise spectra (Tables 1 and 2). The OPR can be retrieved from ν_2 band spectra obtained at low resolving power because several para lines are well separated in wavelength from strong ortho lines (Fig. 2). The band regions most sensitive to the OPR lie at 6.12 and 6.4 μm . At 6.12 μm , emission is dominated by the $1_{11}-0_{00}$ para line, and three other significant para lines (Fig. 2). Since the nearby 6.05 and 6.18 μm peaks are mainly due to ortho lines ($2_{12}-1_{01}$ and $1_{10}-1_{01}$, respectively), the intensity ratios $I(6.12\mu\text{m})/I(6.18\mu\text{m})$ and $I(6.12\mu\text{m})/I(6.05\mu\text{m})$ increase with decreasing OPR. Similarly, at 6.4 μm , the contributions from para lines ($0_{00}-1_{11}$ and $1_{11}-2_{02}$) dominate the spectrum and the intensity ratio $I(6.4\mu\text{m})/I(6.5\mu\text{m})$ is a function of the OPR. The variation in water ν_2 band features with OPR, for $T_{rot} = 30$ K, at the *Spitzer* IRS spectral resolution is illustrated in Fig. 7. From the models depicted in this figure, the peak intensities of the 6.05 μm , 6.18 μm , and the 6.50 μm features increase by $\approx 8\%$, $\approx 8\%$, and $\approx 13\%$ respectively as the OPR changes from values of 2 to 3. The intensity at 6.12 and 6.4 μm decreases in turn by $\approx 18\%$. However, the 6.64 and 6.85 μm water features remain constant and their intensity ratio only depends upon T_{rot} . The different behaviors of the intensity of the features with T_{rot} and OPR make the accurate measurement of these two parameters possible.

For the comet C/2003 K4 (LINEAR) spectrum at position A, 7.2'' offset from the nucleus position (Fig. 1), we obtain an $\text{OPR} = 2.47 \pm 0.27$ when fitting the entire water spectrum (Table 2). The other spectra yield OPRs consistent with this value (Tables 1, 2). Conversions between ortho to para states by radiative transitions or by collisions in the coma have very low probability. The constancy of the OPR in the coma also has been convincingly demonstrated in comet C/2004 Q2 (Machholz) by Bonev et al. (2007). The weighted mean of all OPR values in comet C/2003 K4 (LINEAR) given in Table 2 (fits to 5.8–7.0 μm region)

is 2.43 ± 0.15 . The OPR value derived for the aperture slit closest to the nucleus (labeled A), 2.47 ± 0.27 , corresponds to a spin temperature $T_{spin} = 28.5^{+6.5}_{-3.5}$ K.

The reduced χ^2 between 5.8 and 7.1 μm obtained for the spectrum at 7.2'' offset is 0.5. When the OPR is fixed to $\text{OPR} = 3$, the reduced χ^2 is $\simeq 15\%$ higher (45% higher when fitting 6.3–7 μm partial spectrum). Figure 8 shows the model fit obtained in this case which yields $T_{rot} = 30.5 \pm 3.3$ K, a value close to that obtained with $\text{OPR} = 2.47$ (Table 2). There is significantly higher discrepancy between 6.3 and 6.4 μm in the two models.

The OPR (and T_{rot}) determination relies on the assumption that water emission dominates the 5.8–7.2 μm C/2003 K4 (LINEAR) spectrum. Misleading results can be obtained when extra emission from other constituents is present. In addition to the 6 μm residual emission discussed in § 3.2, PAH emission peaks (e.g., Peeters et al. 2002) near 6.2 μm , i.e., in the region where the shape of H₂O band depends on the OPR (Fig. 8). Because the independent model fits of partial subsections of the spectra provide consistent OPR values (Table 2), our OPR determinations are likely not affected by unaccounted species. We also conclude that the dominant source of emission in the SL2 wavelength regime for comet C/2003 K4 (LINEAR) is the water ν_2 band.

Our derived water OPR for C/2003 K4 (LINEAR) is comparable to values derived for Oort Cloud (nearly-isotropic) comets such as C/1995 O1 (Hale-Bopp), C/1999 H1 (Lee), C/1999 S4 (LINEAR), C/2001 Q1 (NEAT), and C/2001 A2 (LINEAR), although lower ($\sim 15\text{--}20\%$) than that reported for Jupiter-family (ecliptic) comets, for example 103P/Hartley 2 or 1P/Halley (Crovisier et al. 2000; Dello Russo et al. 2005; Kawakita et al. 2006) or C/2004 Q2 (Machholz) (Bonev et al. 2007). The value of $T_{spin} = 28.5^{+6.5}_{-3.5}$ K for C/2003 K4 (LINEAR) is suggestive of precometary ice formation in a cold molecular cloud environment devoid of secondary processing in a warm solar nebula (Kawakita et al. 2006), although the precise interpretation of the OPR as a probe of the primordial formation zones of comets in the protosolar nebula remains vexing (Crovisier 2007). We also do not have spectroscopic measurements of other common cometary ices such as ammonia or methane in coma of C/2003 K4 (LINEAR). Thus we are unable to ascertain whether the ices incorporated into the nucleus of C/2003 K4 (LINEAR) share the same chemical composition and homogeneity of T_{spin} as that found for other comets of diverse dynamical classes (Crovisier 2007).

3.5. Water Production Rate

The intensity of the ν_2 band measured for C/2003 K4 along the nine slit extractions is given in Table 1, and is plotted as a function of offset in Fig. 9. The evolution with

distance to nucleus is consistent with that computed using a Haser distribution for the water density and $Q(\text{H}_2\text{O}) = (2.43 \pm 0.25) \times 10^{29} \text{ molec. s}^{-1}$, where the error includes a 10% uncertainty in the IRS absolute calibration (Spitzer Science Center 2006). Some deviations are observed, which may be related to asymmetries in the density distribution and/or (for the noisy spectra) incorrect background subtraction.

The derived pre-perihelion ($r_h = 1.76 \text{ AU}$) water production rate is consistent with OH 18-cm observations performed with the Nançay radio telescope which yield $Q(\text{H}_2\text{O}) \sim 2 \times 10^{29} \text{ molec. s}^{-1}$ at the epoch of the *Spitzer* observations (Crovisier et al., personal communication). Post-perihelion measurements obtained from H_2O 557 GHz line observations using the Odin satellite give a $Q(\text{H}_2\text{O})$ about a factor of two lower at $r_h = 1.7\text{--}1.8 \text{ AU}$ (Biver et al. 2007), which suggests a pre/post-perihelion asymmetry in the gaseous activity of the comet. Similar asymmetrical perihelion production rates of water and other volatiles has been observed in other comets, including C/1995 O1 (Hale-Bopp) (e.g., Fig. 3 of Biver et al. 1997) and possibly 1P/Halley (e.g., Fig. 6 of Gehrz et al. 2005).

4. Residual Emission Between 5.5 and 7.6 μm

Lisse et al. (2006) report emission from carbonate minerals at 6.5–7.2 μm and organic (PAH) emission at 6.2 μm in the spectrum of comet 9P/Tempel after collision with the *Deep Impact* impactor. In a subsequent paper, Lisse et al. (2007) claim the detection of these emission features in the ISO spectrum of comet C/1995 O1 (Hale-Bopp) published by Crovisier et al. (1997b). However, a re-analysis of the ISO observations of comet Hale-Bopp by Crovisier & Bockelée-Morvan (2007) does not confirm the detection of PAHs reported by Lisse et al. (2007). Furthermore, Crovisier & Bockelée-Morvan (2007) demonstrate that carbonate emission at 7 μm , though possibly marginally present, is fainter by a factor 2 to 3 than asserted by Lisse et al. (2007). Figure 8 shows representative spectra of PAHs and carbonate minerals compared to the best *Spitzer* spectrum of comet C/2004 K4 (LINEAR). Our synthetic water spectrum wholly accounts for any emission in-excess of the continuum at the wavelengths of PAHs and carbonate emission. As discussed in § 3.1 and § 3.2, residual emission is only marginally present in some spectra near 5.9 and 6.05 μm in various apertures in the C/2003 K4 (LINEAR). Since PAH features are narrow ($\Delta\lambda \sim 0.15 \mu\text{m}$) and peak near the water 6.18 μm pattern, a significant contribution of PAHs in the spectrum would have resulted in an intensity ratio $I(6.18 \mu\text{m})/I(6.05 \mu\text{m})$ higher than observed. Similarly, carbonate emission, if present, would have been seen directly on the original spectra (continuum background included, Fig. 3) longward of 7 μm . Indeed the 3- σ upper limit to the peak intensity of any carbonate or PAH emission, computed from the residual emission

between 6.15 to 6.30 μm and 6.75 to 7.25 μm using the representative PAH and carbonate spectra shown in Fig. 8, does not exceed 7 to $8 \times 10^{-21} \text{ W cm}^{-2} \mu\text{m}^{-1}$ ($\lesssim 10^{-3} \text{ Jy}$) in the C/2003 K4 (LINEAR) spectrum at 7.2'' offset position.

As depicted in Fig. 10, *Spitzer* spectra of comets C/2004 B1 (LINEAR), 71P/Clark, and 9P/Tempel 1 show evidence for ν_2 water emission arising from sublimating ices in their comae. A detailed study, similar to that presented in this paper, is required to investigate whether emission from other compounds is present in these spectra (Woodward et al. 2007).

From Fig. 8, we see that a narrow ($\Delta\lambda \sim 0.1 \mu\text{m}$) residual emission feature is present near $\sim 7.3 \mu\text{m}$ (1370 cm^{-1}). A small spectral segment of the *Spitzer* IRS data near $7.3 \mu\text{m}$, shown in Fig. 11, provides detailed, close-up view of this emission feature. The origin of this feature is unclear. The peak flux and integrated feature flux is in excess of that anticipated from spurious fringe signal power. A possible candidate is emission from the $\text{SO}_2 \nu_3$ band at $7.34 \mu\text{m}$ that has a fluorescence emission rate at 1 AU from the Sun of $6.6 \times 10^{-4} \text{ s}^{-1}$ (Crovisier 2002). Synthetic spectra of $\text{SO}_2 \nu_3$ band obtained using the HITRAN database (Rothman et al. 2004) approximately match the width of the feature, but the central wavelengths do not coincide. In addition, the measured intensity in the spectrum obtained at 7.2'' offset in the coma of comet C/2003 K4 (LINEAR), $\simeq 10^{-21} \text{ W cm}^{-2}$, would imply a $\text{SO}_2/\text{H}_2\text{O}$ production rate ratio of 2.5%, a factor 10 times higher than measured in comet C/1995 O1 (Hale-Bopp) (Bockelée-Morvan et al. 2000). Therefore, it seems unlikely that the observed $7.3 \mu\text{m}$ feature is due to SO_2 . The NIST database² provides band positions of a number of gas phase species, including organics. No satisfactory candidate could be found. For example, methyl formate HCOOCH_3 , identified in cometary atmospheres (Bockelée-Morvan et al. 2000), has a band of medium strength at 1371 cm^{-1} , but also a much stronger band at 1754 cm^{-1} ($5.7 \mu\text{m}$) which is not seen in the *Spitzer* spectra. Acetic acid exhibits a strong band at 1375 cm^{-1} , but a still stronger one at 1248 cm^{-1} ($6.94 \mu\text{m}$). If the feature is originating from a gas phase species, then the abundance of this molecule relative to water should be on the order of 1% or more, based on the measured intensity and typical fluorescence emission rates in cometary environment.

The $7.3 \mu\text{m}$ wavelength corresponds to the characteristic vibrational frequency of the CH_3 “umbrella” deformation mode ($\sim 1375 \text{ cm}^{-1}$). A $7.3 \mu\text{m}$ absorption feature has been detected in some galactic and extragalactic sources (e.g., Chiar et al. 2000; Spoon et al. 2000), and assigned to aliphatic hydrocarbons. However, an absorption signature at $6.85 \mu\text{m}$ is also observed, corresponding to CH_2 bending vibrations. Spectra of various carbonaceous refractory materials, including chondritic material, that contain aliphatic chains show that

²<http://webbook.nist.gov/chemistry/>

these two features are present as a doublet with intensity ratio $I(6.8\mu\text{m})/I(7.3\mu\text{m}) > 1$ (Pendleton & Allamandola 2002). In contrast, no residual emission is observed at $6.8\mu\text{m}$ in the comet C/2003 K4 (LINEAR) spectrum. Therefore, aliphatic hydrocarbons are not likely the source of the cometary $7.3\mu\text{m}$ feature, although such compounds have been identified in the material captured from comet 81P/Wild 2 by the Stardust spacecraft (Keller et al. 2006).

A few galactic and extragalactic sources exhibit a weak emission feature at $7.3\text{--}7.4\mu\text{m}$ (with no $6.85\mu\text{m}$ counterpart) that shows up on the wing of the well known strong $7.7\mu\text{m}$ complex attributed to CC stretching/CH in plane bending vibrations of aromatics (likely PAHs) compounds (Peeters et al. 2002). Based on theoretical calculations of expected CC stretching band positions of PAHs of various complexity (see Peeters et al. 2002), this weak component is likely a PAH signature. However, the comet feature may have a different origin as no strong 6.8 and $7.7\mu\text{m}$ PAH emission is evident in the *Spitzer* spectra of C/2003 K4 (LINEAR).

5. CONCLUSIONS

We have observed the ν_2 vibrational band of water in comet C/2003 K4 (LINEAR) within 5.5 to $7.6\mu\text{m}$ *Spitzer* IRS spectra, deriving a water production rate of $(2.43 \pm 0.25) \times 10^{29}$ molec. s^{-1} when the comet was at a pre-perihelion heliocentric distance of 1.760 AU. Although the IRS spectra are of moderate resolution, modeling of the observed emission in the 5.7 to $6.8\mu\text{m}$ region constrained the water spin temperature to be $28.5^{+6.5}_{-3.5}$ K. The measured T_{spin} is comparable to that of other Oort cloud comets and suggestive of a common formation zone for the precometary water ices that eventually agglomerated into the nuclei, though the precise interpretation of the OPR as a probe of the primordial formation zones of comets in the protosolar nebula remains controversial (Crovisier 2007). The observed decrease (at $3\text{-}\sigma$ confidence level) of the water rotational temperature with cometocentric distance is compatible with evolution from thermal to fluorescence equilibrium and constrains somewhat the role of electron collisions in water excitation. The kinetic temperature of the gas is poorly constrained.

Neither emission from carbonates nor PAHs was necessary to account for any emission in excess of the continuum at wavelengths between 5 to $7\mu\text{m}$, suggesting that these species are not present in the coma of C/2003 K4 (LINEAR) at the abundance levels measured by Lisse et al. (2006) in comet 9P/Tempel 1. However, an emission feature at $\sim 7.3\mu\text{m}$ is observed that remains unidentified, as potential emission candidates, the SO_2 ν_3 band or CH_3 deformation modes, can be discounted.

This work is based on observations made with the *Spitzer* Space Telescope, which is operated by the Jet Propulsion Laboratory, California Institute of Technology under a contract with NASA. Support for this work was provided by NASA through an award issued by JPL/Caltech. Support for this work also was provided by NASA through contracts 1263741, 1256406, and 1215746 issued by JPL/Caltech to the University of Minnesota. C.E.W. and M.S.K. acknowledge support from the National Science Foundation grant AST-037446. M.S.K. acknowledges support from the University of Minnesota Doctoral Dissertation Fellowship. The authors also wish to thank E. F. Polomski with initial assistance in planning PID 131 activities, J. Crovisier for useful discussions, E. Peeters for providing her PAH spectra in digital form, and the referee who helped improve the discussion presented in the manuscript.

Facilities: Spitzer (IRS)

REFERENCES

- A’Hearn, M. F., et al. 2005, *Science*, 310, 258
- Barber, R. J., Tennyson, J., Harris, G. J., & Tolchenov, R. N. 2006, *MNRAS*, 368, 1087
- Belton, M. J. S., et al. 2006, *Icarus* in press
- Bensch, F., & Bergin, E. A., 2004, *ApJ*, 615, 531
- Bernard Salas, J., Pottasch, S. R., Beintema, D. A., & Wesselius, P. R. 2001, *A&A*, 367, 949
- Biver, N., 1997, PhD thesis, University of Paris 7
- Biver, N., et al. 2007, *P&SS*, in press
- Biver, N., et al. 2007, *Earth, Moon, & Planets*, 78, 5
- Bockelée-Morvan, D., 1987, *A&A*, 181, 169
- Bockelée-Morvan, D., & Crovisier, J. 1989, *A&A*, 216, 278
- Bockelée-Morvan, D., et al. 2000, *A&A*, 353, 1101
- Bockelée-Morvan, D., Crovisier, J., Mumma, M. J., & Weaver, H. A. 2004, in *Comets II*, eds. M. Festou, H. U. Keller, and H. A. Weaver, (University of Arizona Press: Tucson), p.391
- Bonev, B. P., Mumma, M. J., Villanueva, G. L., Disanti, M. A., Ellis, R. S., Magee-Sauer, K., & Dello Russo, N. 2007, *ApJ*, 661, L97
- Bonev, B. P., Mumma, M. J., Disanti, M. A., Dello Russo, N., Magee-Sauer, K., Ellis, R. S., & Stark, D. P. 2006, *ApJ*, 653, 774
- Capria, M. T. 2002, *Earth, Moon, & Planets*, 89, 161
- Capria, M. T., et al. 2000, *A&A*, 357, 359
- Chiar, J. E., Tielens, A. G. G. M., Whittet, D. C. B., Schutte, W. A., Boogert, A. C. A., Lutz, D., van Dishoeck, E. F., & Bernstein, M. P. 2000, *ApJ*, 537, 749
- Crovisier, J., 1989, *A&A*, 213, 459
- Crovisier, J. 2002, Constants for molecules of astrophysical interest in the gas phase: photodissociation, microwave and infrared spectra. <http://www.lesia.obspm.fr/~crovisier/basemole>

- Crovisier, J. 2007, arXiv:astro-ph/0703785
- Crovisier, J., & Bockelée-Morvan D. 2007, *Icarus* (in press)
- Crovisier, J., et al. 2002, in *Thermal Emission Spectroscopy and Analysis of Dust*, ASP Conf. Ser. 196, eds. Y. Pendelton, D. Cruikshank [ASP: San Francisco], 109
- Crovisier, J., et al. 1997a, *First ISO Workshop on Analytical Spectroscopy*, ESA SP 419, 137
- Crovisier, J., et al. 1997b, *Science* 275, 1904
- Dello Russo, N., Bonev, B. P., DiSanti, M. A., Mumma, M. J., Gibb, E. L., Magee-Sauer, K., Barber, R. J., & Tennyson, J. 2005, *ApJ*, 621, 537
- Dello Russo, N., DiSanti, M. A., Magee-Sauer, K., Gibb, E. L., Mumma, M. J., Barber, R. J., & Tennyson, J. 2004, *Icarus*, 168, 186
- Eberhardt, P., & Krankowsky, D. 1995, *A&A*, 295, 795
- Ehrenfreund, P., et al. 2004, in *Comets II*, eds. M. Festou, H. U. Keller, and H. A. Weaver, (University of Arizona Press: Tucson), p.115
- Gehrz, R. D., Roellig, T. L., Werner, M. W., Fazio, G. G., Houck, J. R., Low, F. J., Rieke, G. H., Soifer, B. T., Levine, D. A., & Romana, E. A. 2007, *Rev. Sci. Instr.*, 78, 011302
- Gehrz, R. D., Hanner, M. S., Homich, A. A., & Tokunaga, A. T. 2005, *AJ*, 130, 2383
- Gunnarsson, D., et al. 2003, *A&A*, 402, 383
- Harker, D. E., Woodward, C. E., Wooden, D. H., Trujillio, C., & Fisher, S. 2007, *Icarus*, in press
- Jacquinet-Husson, N., et al. 2005, *JQRST*, 95, 429
- Houck, J. R., et al. 2004, *ApJS*, 154, 18
- Kawakita, H., et al. 2006, *ApJ*, 643, 1337
- Keller, L. P., et al. 2006, *Science*, 314, 1728
- Kelley, M. S., et al. 2006, *ApJ*, 651, 1256
- Lisse, C. M., Kraemer, K. E., Nuth, J. A., Li, A., & Joswiak, D. 2007, *Icarus* 187, 69
- Lisse, C. M., et al. 2006, *Science*, 313, 635

- Markwick, A. J. & Charnley, S. B. 2005, in *Highlights of Astronomy*, Vol. 13, eds. O. Engvold, (Astron. Soc. Pacific: San Francisco) p.518
- Meech, K. & Svoren, J. 2004, in *Comets II*, eds. M. Festou, H. U. Keller, and H. A. Weaver, (University of Arizona Press: Tucson), p.317
- Mumma, M. J., et al. 2003, *Adv. Space Res.*, 31, 2563
- Mumma, M. J., Weissman, P. R., & Stern, S. A. 1993, *Protostars and Planets III*, eds. M. H. Levy and J. I. Lunine, (University of Arizona Press: Tucson), p.1177
- Oró, J., Lazcano, A., & Ehrenfreund, P. 2006, in *Comets and the Origin and Evolution of Life*, eds. P. J. Thomas, R. D. Hicks, C. F. Chyba, C. P. McKay (Springer: New York), p.1
- Partridge, H., & Schwenke, D. W. 1997, *J. Chem. Phys.*, 109, 4618
- Peeters, E., Hony, S., Van Kerckhoven, C., Tielens, A. G. G. M., Allamandola, L. J., Hudgins, D. M., & Bauschlicher, C. W. 2002, *A&A*, 390, 1089
- Pendleton, Y. J., & Allamandola, L. J. 2002, *ApJS*, 138, 75
- Prialnik, D., Benkhoff, J., & Podolak, M. 2004, in *Comets II*, eds. M. Festou, H. U. Keller, and H. A. Weaver, (University of Arizona Press: Tucson), p.359
- Prialnik, D. 2002, *Earth, Moon, & Planets*, 89, 27
- Rothman, L.S., et al. 2005, *JQSRT*, 96, 139
- Russell, R. W., Lim, D. L., Sitko, M. L., & Carpenter, W. J. 2004, *IAUC*, 8361
- Schulz, R., Stüwe, J. A., & Erd, C. 2005, *Earth, Moon, & Planets*, 97, 387
- Sitko, M. L., Russell, R. W., Lynch, D. K., & Lim, D. L. 2004, *IAUC*, 8391
- Smith, J. D. et al. 2007, *PASP*, submitted
- Spitzer* Science Center 2006, *Infrared Spectrograph Data Handbook* (Pasadena: SSC)
http://ssc.spitzer.caltech.edu/irs/dh/dh30_v1.pdf/
- Spoon, H. W. W., Koornneef, J., Moorwood, A. F. M., Lutz, D., & Tielens, A. G. G. M. 2000, *A&A*, 357, 898
- Werner, M. W., et al. 2004, *ApJS*, 154, 1

- Wooden, D. H., et al. 2005, in Comets II, eds. M. Festou, H. U. Keller, and H. A. Weaver, (University of Arizona Press: Tucson), p.33
- Woodward, C.E., Kelley, M. S., Bockelée-Morvan, D., et al. 2007, in preparation
- Woodward, C. E., Kelley, M. S., & Wooden, D. H. 2004, IAUC, 8131
- Xie, X., & Mumma, M.J., 1992, ApJ, 386,720
- Young, J. & McGaha, J. 2004, IAUC, 8131
- Zakharov,V., et al., 2007, A&A, in press

Table 1. WATER IN C/2003 K4 (LINEAR): MODEL FITS

Extraction Slit ID	Offset ^a (")	Offset ^a (km)	Band Intensity ^b (10^{-20} W cm $^{-2}$)	T_{rot} ^c (K)	OPR ^c	χ^2_{ν} ^{c,d}
A 0-27	7.2	7377	5.51 ± 0.16	33.5 ± 4.0	2.47 ± 0.30	0.5
B 0-22	12.9	13198	2.67 ± 0.10	28.6 ± 3.6	2.47 ± 0.34	1.0
C 0-17	21.3	21785	1.62 ± 0.09	22.8 ± 4.3	2.5 ^e	1.6
D 1-27	14.4	14682	2.88 ± 0.10	27.6 ± 3.5	2.13 ± 0.31	0.5
E 1-22	18.0	18348	1.93 ± 0.09	20.9 ± 3.5	2.56 ± 0.47	1.5
F 1-17	24.7	25229	1.19 ± 0.09	24.8 ± 5.6	2.5 ^e	1.6
G 2-27	21.7	22154	1.68 ± 0.08	22.4 ± 4.2	2.61 ± 0.31	0.9
H 2-22	24.2	24750	1.46 ± 0.08	23.2 ± 4.3	2.38 ± 0.48	1.5
I 2-17	29.6	30209	1.02 ± 0.09	17.7 ± 5.0	2.5 ^e	2.4

^aRelative to the comet C/2003 K4 (LINEAR) ephemeris position derived from JPL #96.

^bBand intensity above fitted continuum between 5.8 and 7.1 μ m.

^cFits to the 6.3–7.0 μ m region.

^dReduced χ^2 between 6.3 and 7.0 μ m ($\chi^2_{\nu} = \chi^2/dof$, with number of degrees of freedom [dof] = 23–3 = 20).

^eAssumed value.

Table 2. WATER IN C/2003 K4 (LINEAR): MODEL FITS USING SEGMENTS

Extraction Slit ID	Regions Fit (μm)	T_{rot} (K)	OPR
A 0-27	5.85 – 7.00	30.7 ± 3.2	2.47 ± 0.27
A 0-27	5.85 – 6.30	36.5 ± 5.8	2.03 ± 0.40
A 0-27	6.30 – 7.00	33.5 ± 4.0	2.47 ± 0.30
B 0-22	5.85 – 7.00	26.5 ± 3.3	2.95 ± 0.40
B 0-22	5.85 – 6.30	59.5 ± 8.8	2.83 ± 0.68
B 0-22	6.30 – 7.00	28.6 ± 3.6	2.47 ± 0.34
D 1-27	5.85 – 7.00	27.0 ± 2.9	2.07 ± 0.24
D 1-27	5.85 – 6.30	42.7 ± 7.6	1.55 ± 0.30
D 1-27	6.30 – 7.00	27.6 ± 3.5	2.13 ± 0.31
G 2-27	5.85 – 7.00	21.4 ± 3.2	2.67 ± 0.41
G 2-27	5.85 – 6.30	54 ± 12	2.16 ± 0.57
G 2-27	6.30 – 7.00	22.4 ± 4.2	2.61 ± 0.31

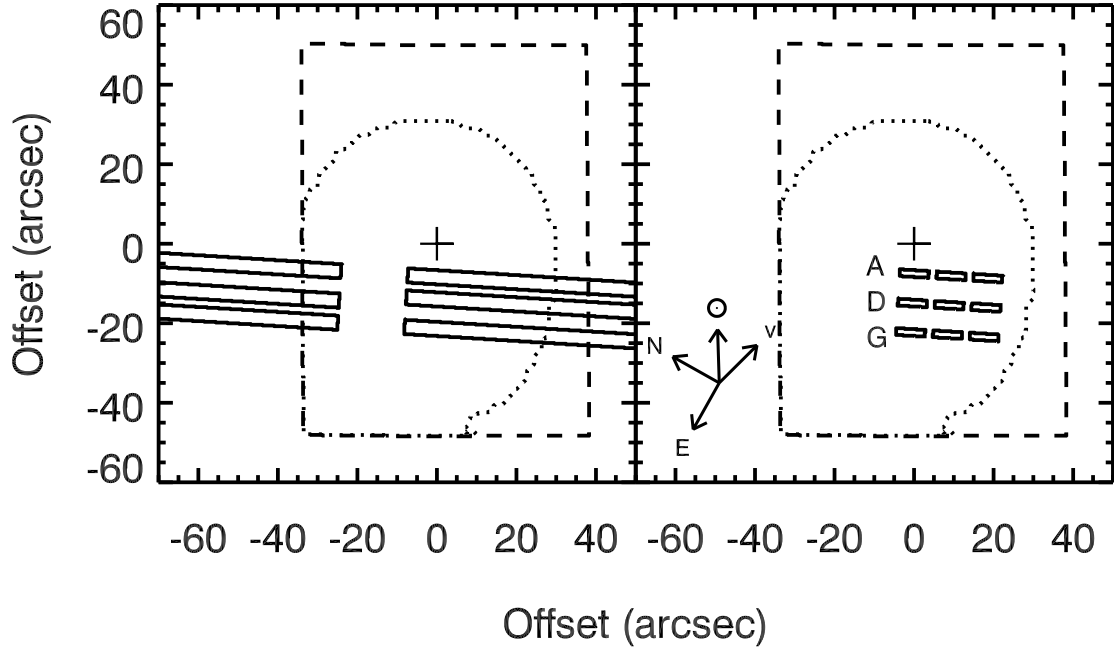


Fig. 1.— **Left:** The 15 μm IRS acquisition image and observed slit positions in comet C/2003 K4 (LINEAR). The *dotted contour* outlines the saturation ellipse in the image and the *dashed line* traces the edge of the peak-up array. The JPL #96 ephemeris position of the comet nucleus is marked with a *cross* (see § 2). The slit positions are outlined with *solid lines*. Celestial north (N) and east (E), the comet’s heliocentric velocity (v), and the direction of the sun (\odot) are marked with *arrows*. **Right:** The nine slit extraction apertures are outlined with *solid lines* and run from left to right, and top to bottom (see Table 1) A, B, C (row 1), D, E, F (row 2), and G, H, I (row 3).

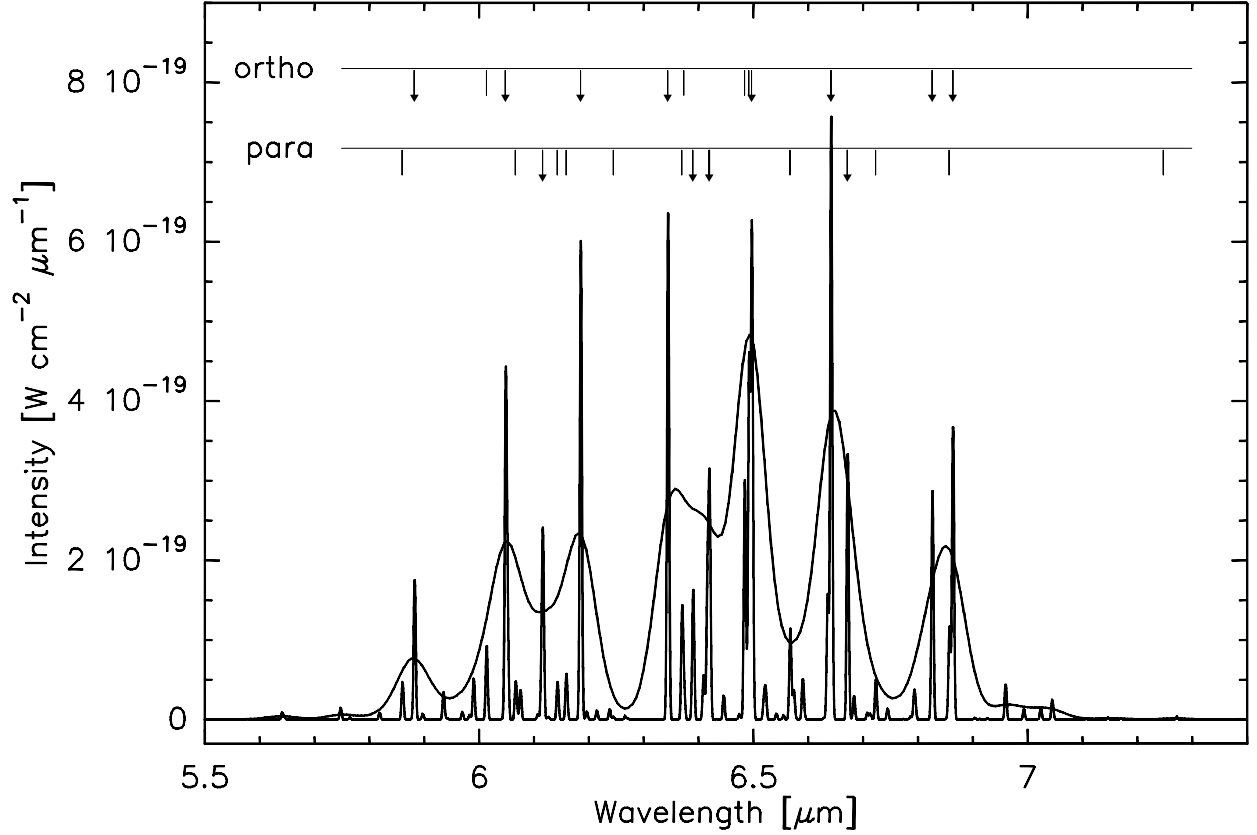


Fig. 2.— Synthetic spectra of the water ν_2 band with a high spectral resolution of $0.0044 \mu\text{m}$ (1 cm^{-1}) with the intensity divided by 5, and at the resolution of $0.065 \mu\text{m}$ corresponding to the *Spitzer* IRS SL2 spectrometer. Ortho and para lines are indicated at the top, with the arrows showing the strongest lines for both spin species. Calculations pertain to a $0.075'$ field of view radius centered on the nucleus position, $Q(\text{H}_2\text{O}) = 5 \times 10^{28} \text{ molec. s}^{-1}$, $r_h = 1.760 \text{ AU}$, $\Delta = 1.409 \text{ AU}$, $v_{\text{exp}} = 0.8 \text{ km s}^{-1}$, $T_{\text{kin}} = 40 \text{ K}$, and $\text{OPR} = 3$.

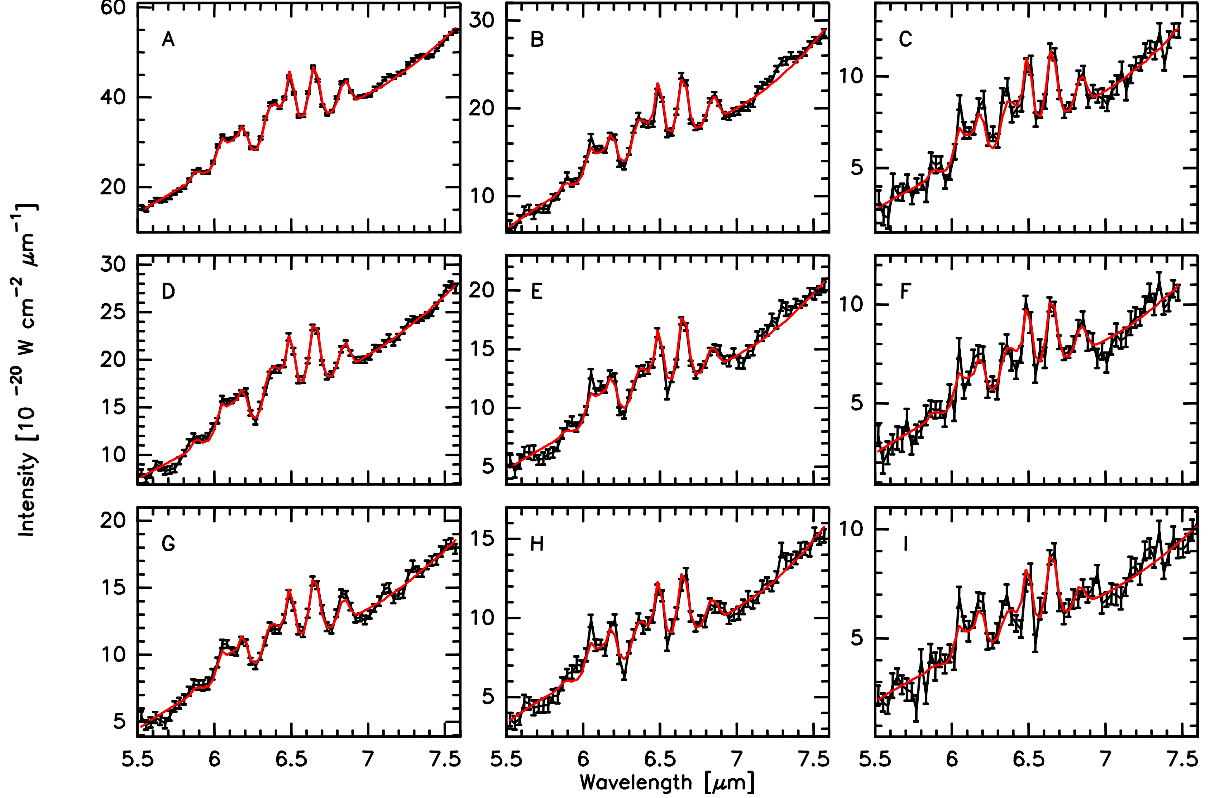


Fig. 3.— Model fits to the spectra of C/2003 K4 (LINEAR) extracted along the slit positions (see § 2, Fig. 1). Capital letters on the top-left corners correspond to the labels defined in the caption of Fig. 1. Data are shown in black with pipeline derived errorbars excluding SL2 fringe uncertainty (see text § 2.1), with the model fits (in red) superimposed. Model fitting was performed with the rotational temperature T_{rot} and the ortho-to-para ratio taken as free parameters. The derived water band intensities are given in Table 1. Derived $T_{rot}(K)$ and OPRs are given in Tables 1 and 2 (see § 3.2). The underlying continuum, described by a polynomial of degree 5 – 6, was also fit simultaneously.

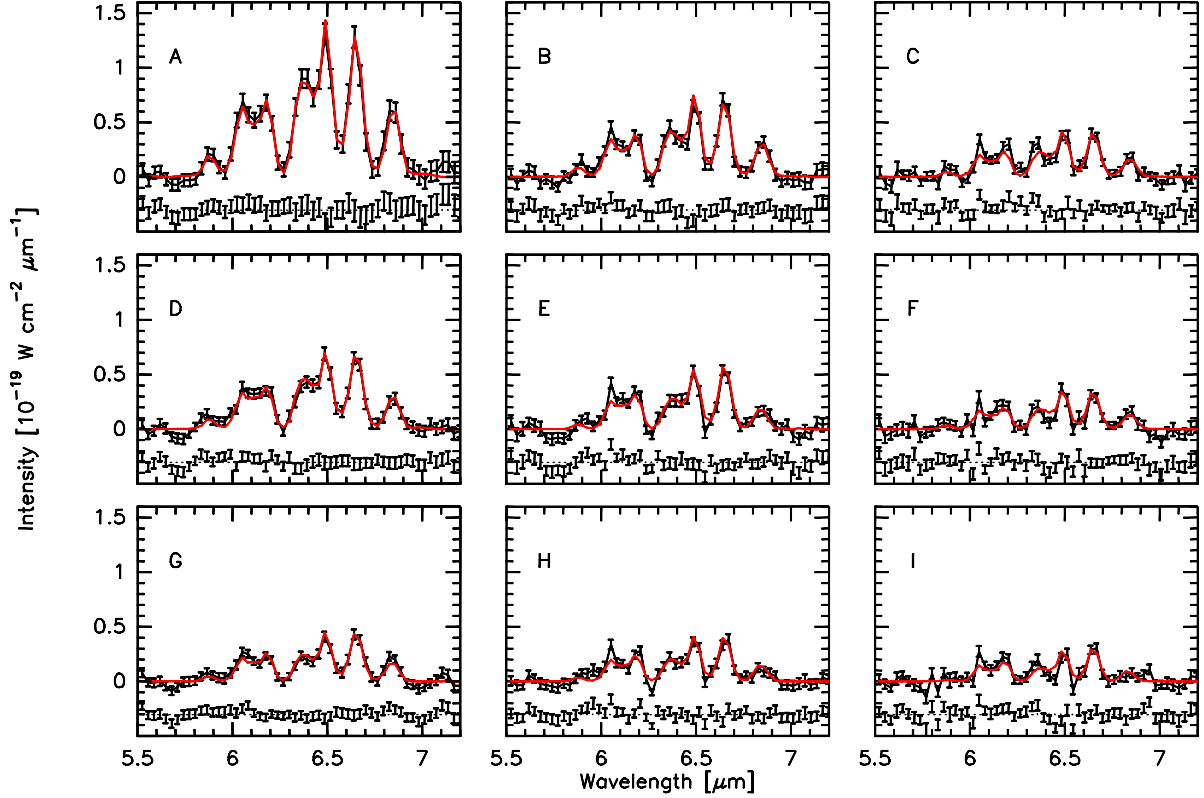


Fig. 4.— Model fits to the spectra of C/2003 K4 (LINEAR)(see § 2, Fig. 1). Same as Fig. 3, with the fitted continuum background subtracted. Data are shown in black with errorbars, with the model fits (in red) superimposed. Errorbars include here SL2 fringe uncertainty (see § 2.1). The residuals are shown on the bottom. Model fitting was performed with the rotational temperature T_{rot} and the ortho-to-para ratio taken as free parameters. The derived values are given in Tables 1 and 2 (see § 3.2).

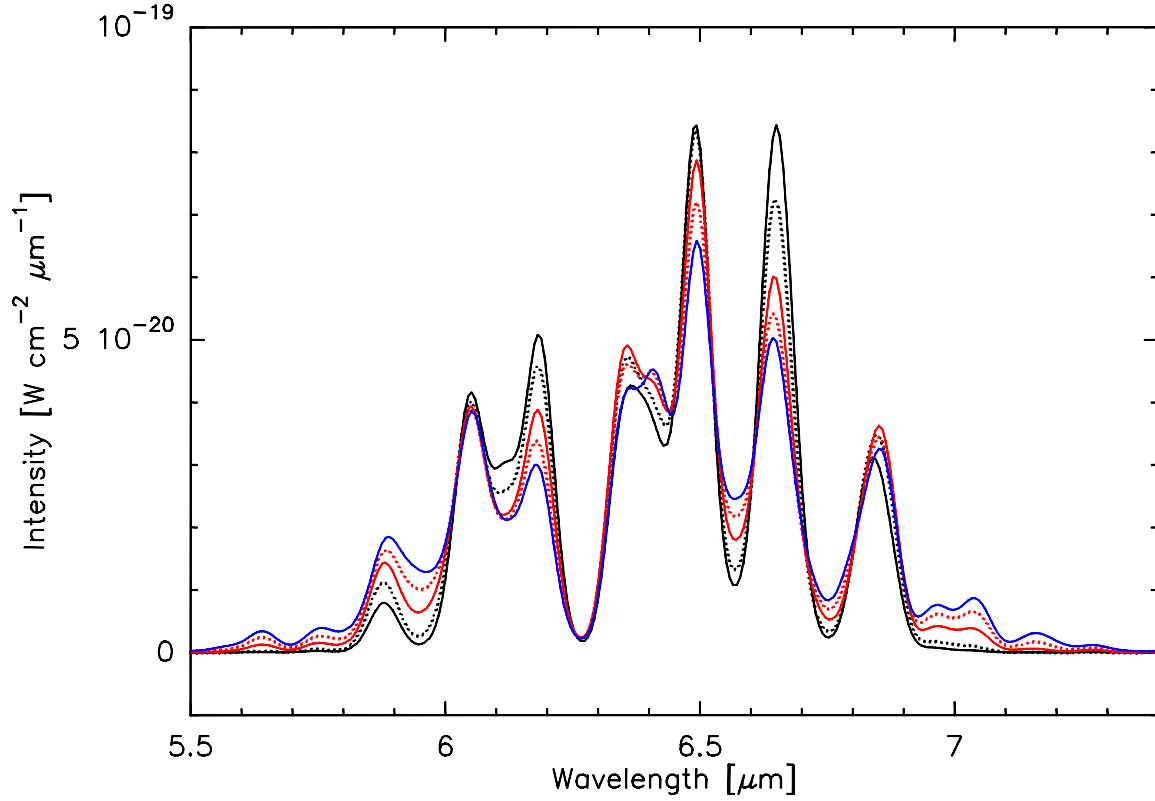


Fig. 5.— Emergent model intensity of the water ν_2 band as a function of rotational temperature, T_{rot} . The synthetic water spectra were generated at the spectral resolution corresponding to the *Spitzer* IRS SL2 spectrometer ($0.065 \mu\text{m}$). Calculations pertain to a $0.075'$ field of view radius centered on the nucleus position, $Q(\text{H}_2\text{O}) = 1 \times 10^{28} \text{ molec. s}^{-1}$, $r_h = 1.760 \text{ AU}$, $\Delta = 1.409 \text{ AU}$, $v_{exp} = 0.8 \text{ km s}^{-1}$, with T_{rot} equal to 20 K (*solid black line*), 30 K (*dotted black line*), 50 K (*solid red line*), 70 K (*dotted red line*), and 90 K (*solid blue line*).

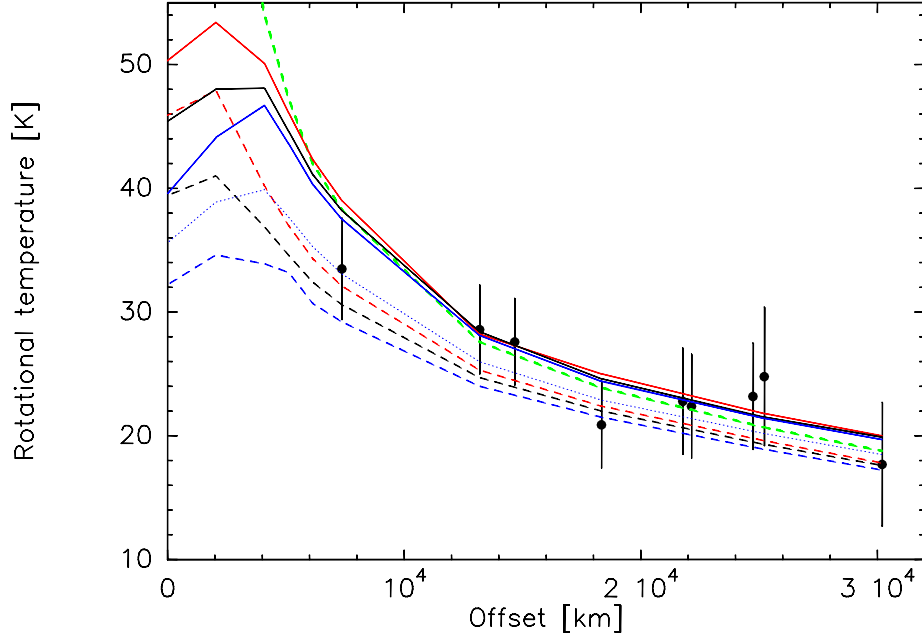


Fig. 6.— Rotational temperature as a function of offset with respect to nucleus position in comet C/2003 K4 (LINEAR). Data points (black dots with errorbars) correspond to the slit extractions shown in Fig 1. Curves show the rotation temperature extracted from synthetic ν_2 spectra computed with a kinetic temperature T_{kin} of 30, 40, 50, and 100 K (*blue*, *black*, *red* and *green* lines, respectively) and different models of the electron density (described by the x_{ne} parameter): $x_{ne} = 1$ (plain lines), $x_{ne} = 0.5$ (dotted lines), $x_{ne} = 0.2$ (dashed lines). For clarity, results obtained with $x_{ne} = 0.5$ are only plotted for $T_{\text{kin}} = 30$ K; for $T_{\text{kin}} = 100$ K, we only show the model output corresponding to $x_{ne} = 0.2$.

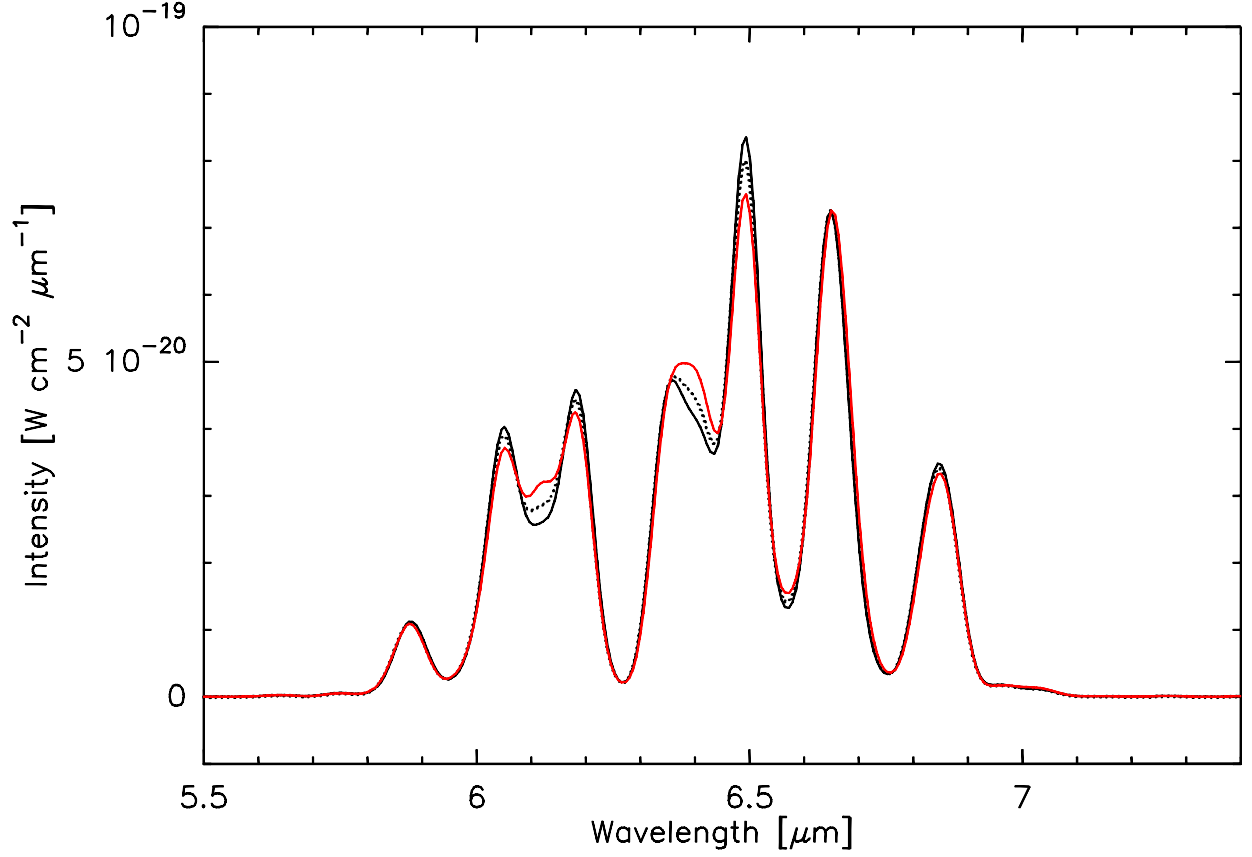


Fig. 7.— Emergent model intensity of the water ν_2 band as a function of the ortho-to-para (OPR) ratio. OPRs of 2.0 (*solid red line*), 2.5 (*dotted black line*), and 3.0 (*solid black line*) are depicted. The synthetic water spectra were generated at the spectral resolution corresponding to the *Spitzer* IRS SL2 spectrometer ($0.065 \mu\text{m}$). Calculations pertain to a $0.075'$ field of view radius centered on the nucleus position, $Q(\text{H}_2\text{O}) = 1 \times 10^{28} \text{ molec. s}^{-1}$, $r_h = 1.760 \text{ AU}$, $\Delta = 1.409 \text{ AU}$, $v_{exp} = 0.8 \text{ km s}^{-1}$, and $T_{rot} = 30 \text{ K}$.

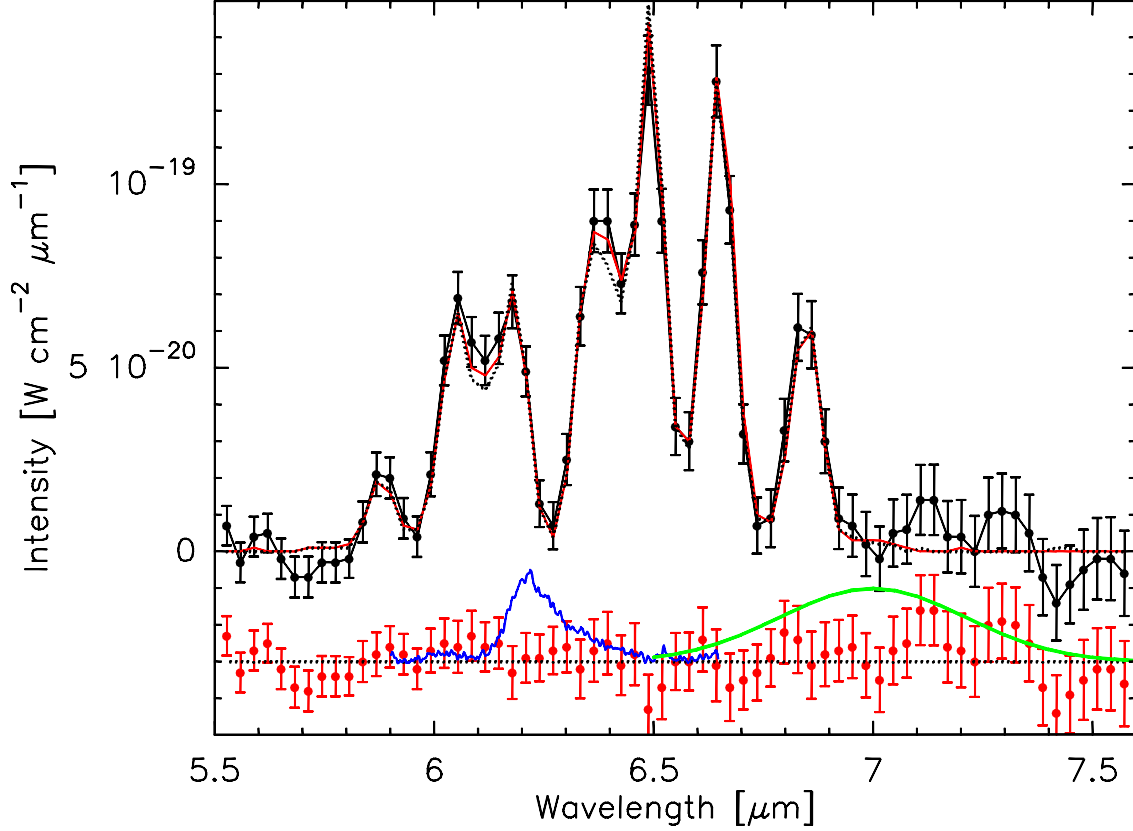


Fig. 8.— Model fits to the spectrum of C/2003 K4 (LINEAR) at $7.2''$ offset from the nucleus. Data are shown in black dots with errorbars that include noise from spectral fringing (see § 2.1). Synthetic spectra with $\text{OPR} = 2.47$ and $\text{OPR} = 3$ are shown in red and in black dotted line, respectively. The former fit was obtained with the OPR set as a free parameter, in contrast to the second fit. The retrieved T_{rot} are 30.7 ± 3.2 K and 30.5 ± 3.3 K, respectively. The residual spectrum from the former fit is shown in red on the bottom, on which are superimposed in arbitrary units an interstellar PAH spectrum typical of class A sources from Peeters et al. (2002) (*blue* spectrum), and a model of carbonate emission from Lisse et al. (2006) (*green* spectrum).

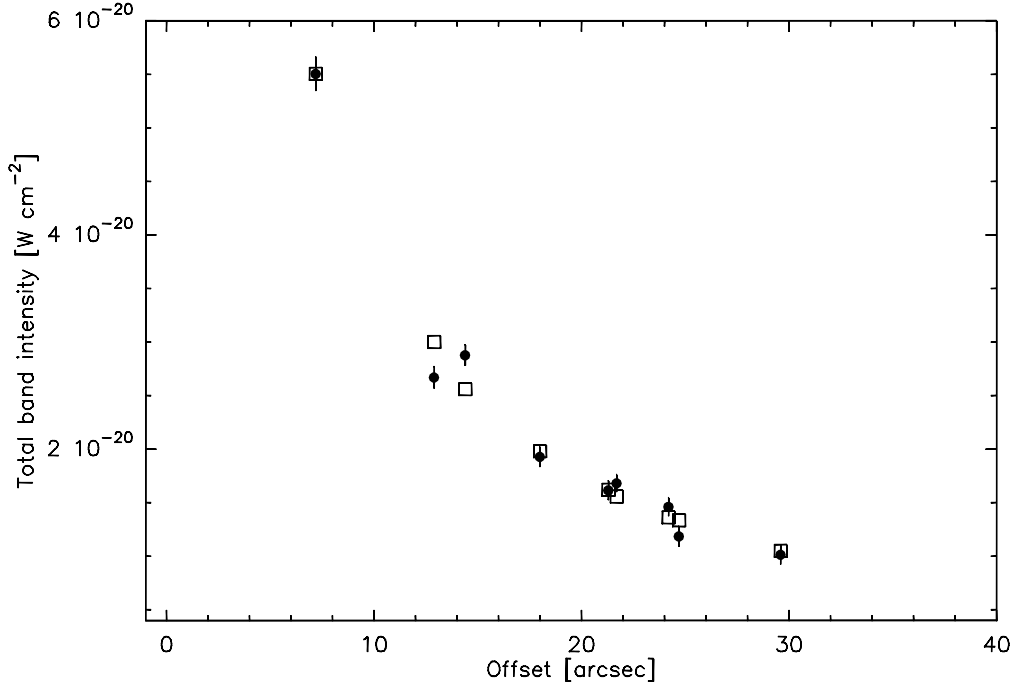


Fig. 9.— Total band intensity between 5.8 and 7 μm in C/2003 K4 (LINEAR) as a function of offset with respect to nucleus position. Data points (black dots with errorbars) correspond to the slit extractions shown in Fig 1. Squares show expected water ν_2 band intensities for $Q(\text{H}_2\text{O}) = 2.43 \times 10^{29} \text{ molec. s}^{-1}$, $v_{exp} = 0.8 \text{ km s}^{-1}$ and $\beta(\text{H}_2\text{O}) = 1.6 \times 10^{-5} \text{ s}^{-1}$ at $r_h = 1 \text{ AU}$.

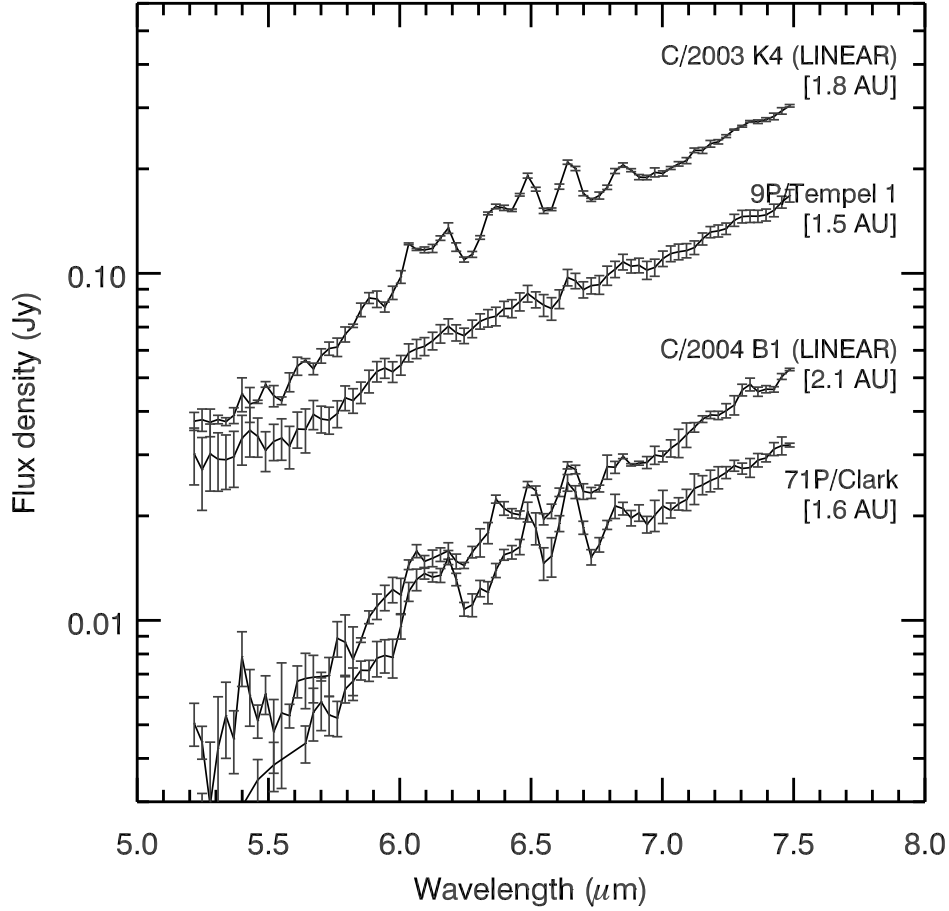


Fig. 10.— A comparison of the ν_2 water bands in Oort Cloud comets C/2003 K4 (LINEAR), C/2004 B1 (LINEAR), and Jupiter-family comets 71P/Clark and 9P/Tempel 1 detected with the *Spitzer* IRS. The data have not been scaled or offset in flux with respect to each other and the spectra do not have the continuum emission removed. Our synthetic model spectrum suggests that water dominates emission in-excess of the continuum at wavelengths between 5.7 and 7 μm .

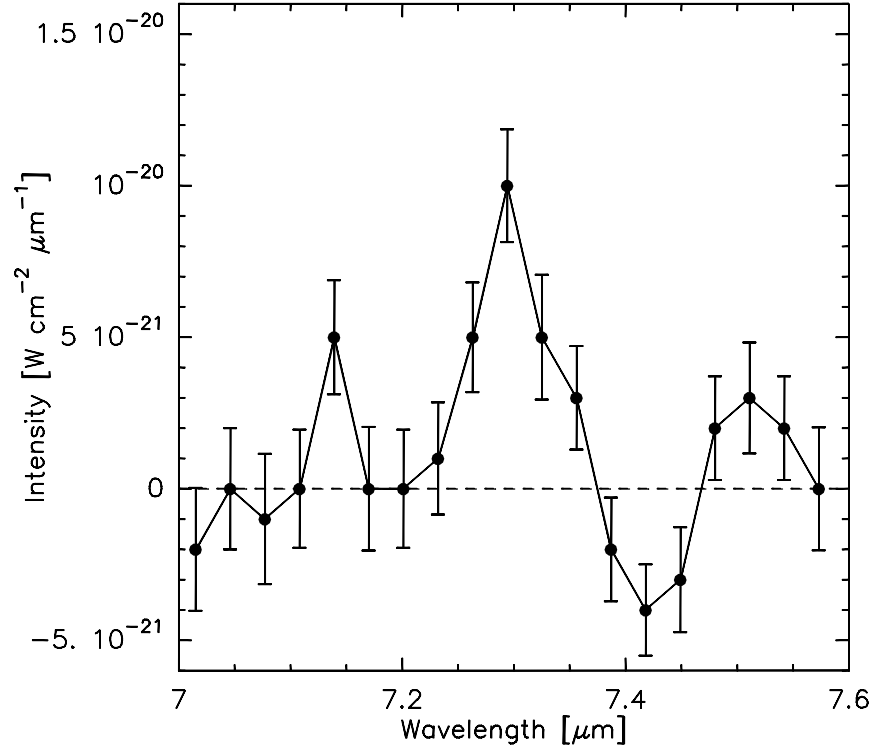


Fig. 11.— Background-subtracted 7–7.6 μm spectrum of C/2003 K4 (LINEAR) showing the detection of a weak emission feature at 7.3 μm . This spectrum has been obtained by averaging slit extractions 0-27, 0-22, 1-27, and 1-22. The uncertainty plotted are the error from extractions of the pipeline reduced individual BCDs and do not include any small excess noise arising from spectral fringing (see § 2.1).